Available online at www.sciencedirect.com
ScienceDirect
Pattern Recognition 40 (2007) 2237–2250
PATTERN RECOGNITION
THE JOURNAL OF THE PATTERN RECOGNITION SOCIETY
www.elsevier.com/locate/pr

A new measure of symmetry and its application to classification of bifurcating structures

David Milner[a], Shmuel Raz[b], Hagit Hel-Or[a,*], Daniel Keren[a], Eviatar Nevo[b]

[a]*Department of Computer Science, University of Haifa, Haifa 31905, Israel*
[b]*Institute of Evolution, University of Haifa, Haifa 31905, Israel*

Received 19 July 2006; accepted 12 December 2006

Abstract

This paper presents a new measure of symmetry for bifurcating structures, which relies not only on topology and ordering, but also on quantitative properties (e.g. length of branches). This measure is based on a specific biological mechanism and on the concept of minimum energy. The effectiveness of the approach is demonstrated in a classification test where leaves taken from plants growing under different stress conditions are classified. Results show that the proposed measure improves classification performance compared to classification based on other leading measures.

Keywords: Symmetry; Bifurcating structures; Graphs; Leaf veins; CSM; Shape characteristics; Continuous symmetry

1. Introduction

Symmetry has long been of interest to people. Symmetry appears in nature as well as in art and other human creations. Weyl [1] introduced bilateral, translatory, rotational and ornamental symmetries from various aspects including art, biology, crystallography and physics and presented mathematical formulations for these symmetry groups. Concentrating on mirror symmetry, Gardner [2] observed symmetry and asymmetry in objects ranging from galaxies to atomic particles.

In this paper, we focus on mirror symmetry of a specific class of structures, namely, bifurcating structures. A 2D object is mirror-symmetric if it is invariant under a reflection about a line (the mirror-symmetry axis). Similarly, invariance under reflection across a plane leads to 3D mirror-symmetry.

The goal of this work is to develop a symmetry measure for bifurcating structures such as veins of plant leaves (Fig. 1B) which can be applied to natural populations. Previous studies on symmetry of bifurcating structures such as graph and tree structures [3–5] considered only topological aspects of the structures. However, given our motivation, the morphological and geometrical aspects of these structures are of crucial importance. In several studies [6,7] measures of symmetry were developed for molecular structures which are considered as 2D and 3D bifurcating structures. These approaches considered the geometry of the structures and the topological connectivity between molecular atoms, but assumed no other constraint on the structures.

In biological systems mirror symmetry forms an important characteristic. Measures of normally distributed deviations from mirror symmetry, known as 'Fluctuating Asymmetry' (FA), is widely used for detecting developmental instability [8]. FA in plant and animal traits has long been known as highly affected by environmental conditions [9,10]. In the last two decades numerous new biological measures were suggested in order to estimate symmetry of single [10] and multiple traits [11–13] within an individual. More advanced methods use morphometric tools, in order to determine FA levels, using landmarks (developmentally homologous points) on the individual body [12,14,15]. Although these methods are used and have been proven to be efficient, they do not consider the specific biological trait developmental mechanism.

* Corresponding author. Tel.: +972 4 8249731; fax: +972 4 8249331.
E-mail addresses: david@tsarfin.com (D. Milner), razshmu@study.haifa.ac.il (S. Raz), hagit@cs.haifa.ac.il (H. Hel-Or), dkeren@cs.haifa.ac.il (D. Keren), nevo@research.haifa.ac.il (E. Nevo).

0031-3203/$30.00
doi:10.1016/j.patcog.2006.12.008

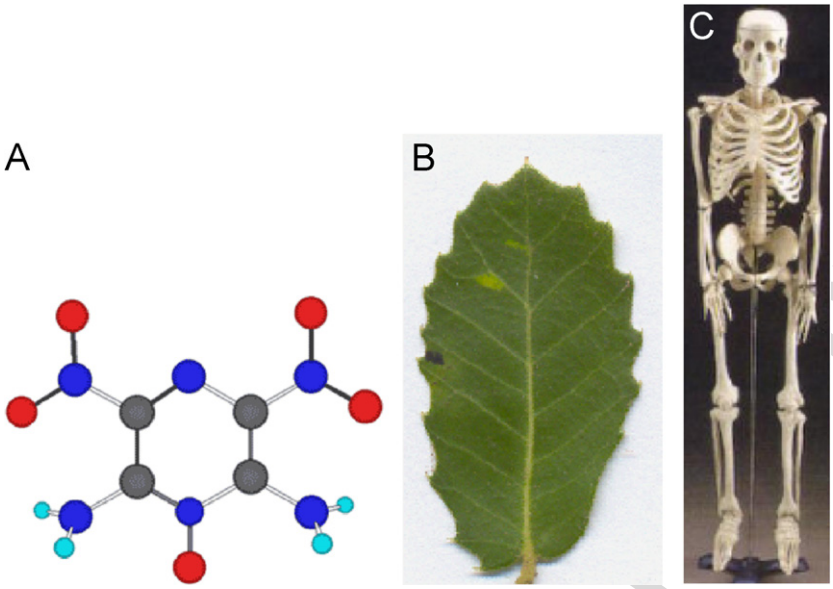

Fig. 1. Examples of bifurcating structures. (A) Molecule. (B) Leaf veins. (C) Human skeleton.

In this work we introduce a novel approach to measuring symmetry of bifurcating structures in which we constrain the topological connectivity of the structures according to biological models. Motivated by an environmental study on the effects of stressful environments on the symmetry of various traits in plants and animals [9,12], the algorithm for measuring the symmetry of bifurcating structures, such as leaf veins, takes into account the biological mechanisms of development and growth [16,17] and relies on nature's laws rather than on arbitrary mathematical models. Following this approach we are able to assert and support the claims of the evolutionary study, that deviation from normal conditions, due to stressful environments affects developmental stability of growth processes manifested in the deviation from perfect symmetry.

We present two measures of symmetry, and provide algorithms for their computation. In both the Local Approach (LoA) and the Global Approach (GoA) for measuring symmetry we evaluate the amount of work (energy) that must be invested to deform a non-symmetric configuration into a perfectly symmetric one. The local approach relates directly to the biological models via elementary deformations. The global approach is based on early work on Continuous Symmetry Measures (CSM) [37]. In Refs. [6,7] symmetry of molecules was measured using the CSM approach, by allowing deformations that preserve the topology of the original structures. In this paper we allow deformations that do not necessarily preserve topological connectivity but that are consistent with biological models of the source structures (in our case veins of leaves).

We further demonstrate the effectiveness of the suggested symmetry measures in a classification test within an evolutionary experiment. Leaves taken from plants growing under different stress conditions are classified to their correct environment. We show that classification based on the proposed symmetry measures improve classification by more than 16% over classification based on leading measures of symmetry. The obtained results show clearly that our measures which are based on the minimum energetic path underlying biological mechanisms yield better separation ability.

2. Previous works

There are two principal questions concerning symmetry: (1) Detection of symmetry—providing a binary decision as to the existence of symmetry in a given object, and, if exists, providing the axes of symmetry. (2) Quantification of symmetry—estimating a measure of the 'amount' of symmetry existing in an object.

Symmetry detection has been studied on various structures including point sets, polygons, 3D objects and grayscale images. Atallah [18] considered the problem of finding mirror symmetry of planar figures consisting of a collection of points, segments, circles, ellipses and other geometric patterns. The input is divided into separate classes of geometrical patterns and symmetry is detected independently in each class. Wolter et al. [19] suggested an algorithm for detecting all exact rotational symmetries in point sets and polygons. Highnam [20] suggested an algorithm for finding all mirror symmetry axes of a planar point set, based on reducing the 2D symmetry problem to a linear pattern-matching problem.

Although efficient, these methods can only detect perfect symmetries and would fail to detect symmetry in symmetric point sets containing even a small amount of noise and perturbations. Alt et al. [21] suggested algorithms for finding symmetry of point sets within R^n in which they introduced the notion of approximate congruence. Saint-Marc and Medioni [22] used contour segments rather then the whole contour as basic features for detection of symmetry. Kuehnle [23] answered

the question of existence of symmetry in a 2D object by reflecting and then comparing the object with the original one. Ogawa [24] detected symmetry using the Hough transform. And Dinggang et al. [25] presented a method for detection of mirror and rotational symmetry of 2D images based on generalized complex moments. Hel-Or et al. [26] performed mirror symmetry analysis of 2D objects and suggested a robust symmetry measure based on rotational features of the object. This measure is not affected by small deviations and occlusions. Kazdan et al. [27] defined a reflective symmetry descriptor of 3D objects as a 2D function. Minovic et al. [29] presented an algorithm for identifying symmetry of an arbitrary 3D object represented by an octree which is robust under noise. Sun and Sherrah [30] used the extended Gaussian image for symmetry detection. The method they presented relies on the observation that in most cases, if the object is symmetric then the extended Gaussian image is symmetric as well. Kazhdan et al. [31] presented the spherical harmonic representation of objects, a rotation invariant representation of spherical functions in terms of the energies at different frequencies.

Numerous methods for detecting symmetry in gray-level images were developed. Sun [32] developed an algorithm that finds mirror symmetry in gray-level images, using gradient information. Marola [33] concentrated on gray-level images and presented a robust symmetry finding algorithm that relies on identification of the centroids of the given image. Zielke et al. [34] presented two symmetry detection methods; the first based on intensity values of an image and the second based on a discrete representation of local orientation. They detected mirror symmetry with respect to a vertical axis. Bigun [35] presented a method to model symmetries of neighborhoods in gray value images, using harmonic functions.

The second principal question concerned with symmetry is symmetry quantification. Buda and Mislov [36] introduced a measure of mirror symmetry based on the Hausdorff distance between sets. Zabrodsky et al. [37] considered symmetry as a continuous feature and introduced symmetry distance that enables both to compare the 'amount' of symmetry between different shapes and the 'amount' of different types of symmetry of the same shape.

Very few studies deal with asymmetry of bifurcating structures (e.g., trees and graphs). Zabrodsky and Weinshall [3] considered the original configuration of points as a graph and reduced the problem of dividing those points into non-empty sets to the classical problem of listing all graph isomorphisms of order 2. Ishikawa et al. [4] considered the problem of object extraction from images and managed the extracted data as tree structures. Tree structures are often related to the symmetry axis representation of shapes as well. By mapping this tree finding problem to a variant of the Steiner Tree problem, it was shown that tree structure detection in images is an NP-complete problem. Despite this fact, an approximate polynomial-time algorithm to the Steiner Tree problem was introduced which is applied after an image has been transformed by a local symmetry mapping. In [6,7] symmetry of molecules was measured using the CSM approach, by allowing deformations that preserve the topology of the original structures.

Numerous measures of symmetry [10–15] were defined and developed within the biology community in an attempt to quantify the dependence of the fluctuating asymmetry of biological systems on environmental conditions [9,10]. Although these methods are used widely and have been proven to be efficient, they can only be used if there is a trivial coupling between object traits. These methods do not consider the specific biological trait developmental mechanism.

In this paper we introduce novel measures of symmetry for bifurcating structures. The measures are constrained to perform within a class of bifurcating structures and are closely related to the mechanisms that create the structures themselves (namely, leaf-venation hypothesis [16,17]).

3. Bifurcating structures—the leaf vein structure

We concentrate on planar bifurcating structures representing veins of leaves. Fig. 1B shows a leaf specimen and Fig. 6A shows the vein structure marked. These structures are assumed to consist of a central main vein which is viewed as the symmetry axis, from which secondary veins bifurcate on both sides. Variations in this structure include differences in the number of secondary veins, their bifurcation points along the main vein, their lengths and their curvature.

In an attempt to quantify deviation from perfect symmetry of these bifurcating structures, it is imperative to understand and take into account the growth process itself that produced the structure. In our case the growth process of leaves. In a recent series of papers, a novel *leaf-venation hypothesis* was introduced [16,17]. We adopt this model as the basis for our study of asymmetry in leaves. A brief summary of this model is given in the following section.

4. Modeling the growth process of leaf veins

The growth hormone, Auxin is the major regulatory shoot signal [16,17] in a leaf, and is responsible for the vein distribution (e.g., density, size and diameter). The leaf veins are made out of phloem bundles [17], through which organic material is transported, and out of xylem which is the pathway for water and soil nutrient. The differentiation of the leaf veins is important, due to the need to supply these nourishing substances to the leaf cells. It must do so as best as possible in the given environment and genome. The *leaf venation hypothesis* [16,17] (Fig. 2—adopted from Ref. [38]) suggests that large water secreting glands called hydathods are the main sites for free auxin synthesis in a leaf. The hydathod sites typically develop along the growing leaf's boundary. A decreasing gradient of free auxin forms from the hydathod site and towards the central leaf area, inducing secondary vein growth (Fig. 2c). The more developed the hydathod [16], with higher free auxin concentration, the smaller the distance between the leaf boundary and the secondary vein termination (i.e. the length of the secondary vein increases—see Fig. 3b). This distance is an important factor in the control of additional vein differentiation and may also regulate the free auxin levels. During the early development stages of the leaf there are gradual shifts of the

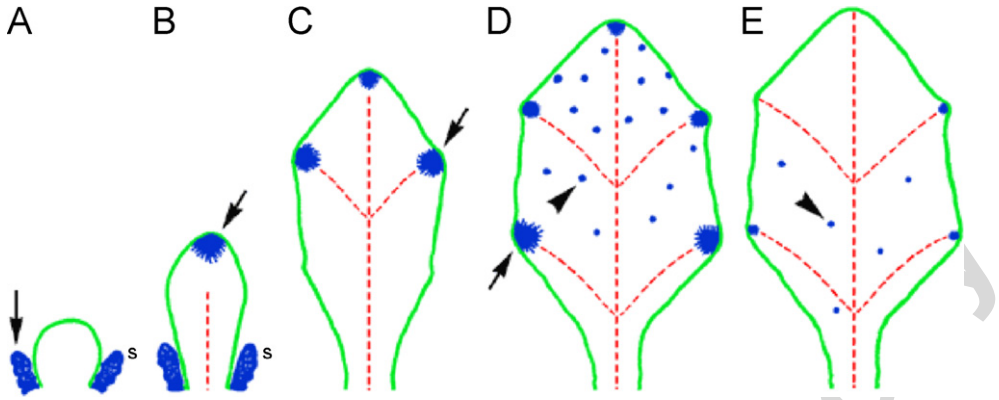

Fig. 2. Leaf venation hypothesis. Schematic diagrams show gradual changes in hydathod sites and free auxin concentration (blue fuzzy blobs) during leaf development in *Arabidopsis*—a flowering plant. Arrows mark the sites with the highest level of free auxin production located at the leaf margin in each developmental stage (A–D), whereas arrowheads show the location of low free auxin (D–E). The ontogeny of central vein and secondary veins is illustrated by broken red lines, while marginal and minor veins are not shown. (A) Early high free auxin production only in the stipules (s) of a very young leaf, before free auxin is detectable in the tip and prior to central vein development. (B) Free auxin production in the tip of a fast growing leaf, illustrating leaf apical dominance and acropetal development of the midvein. (C) High free auxin production in the upper lobes, which induces differentiation of the upper secondary veins. (D) High free auxin production in the lower lobes and randomly distributed sites of secondary free auxin production in the lamina. Secondary veins differentiate below the lower lobes. (E) Maintenance of low free auxin production in lobes and secondary free auxin production in the lamina during a late phase of leaf development (adapted from Ref. [38]).

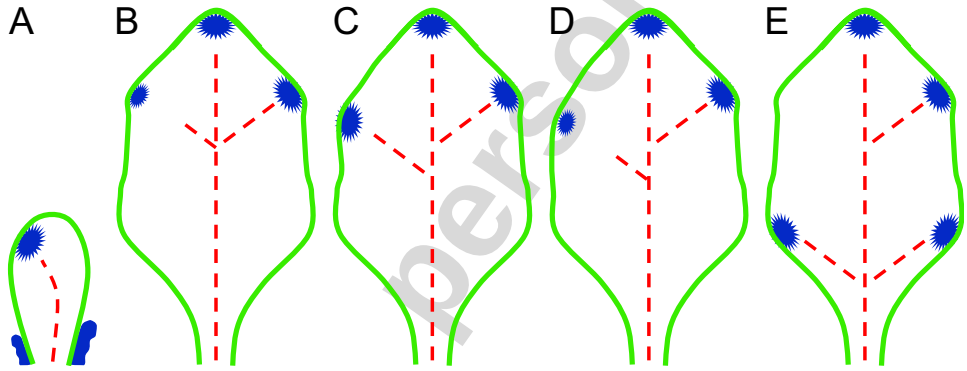

Fig. 3. Deviation from perfect symmetry during leaf development. Schematic diagrams show secondary veins (dashed line) and free auxin concentration sites (blue fuzzy blobs) (A) Asymmetry in auxin concentration in the stipules and in the tip auxin center location induces non-linear growth of the main vein. (B) Unequal free auxin concentration in the upper lobes induces asymmetry in the length of the secondary veins. (C) Misalignment of auxin concentration sites, while maintaining equality of concentration magnitude, induces asymmetric bifurcation points along the main vein. (D) Misalignment of auxin sites, together with unequal auxin concentration, induces asymmetry in the length of the secondary veins as well as asymmetric bifurcation points along the main vein. (E) Extreme asymmetry in auxin concentration may completely prevent bifurcation and growth of a secondary vein, creating unpaired secondary veins. Pairing of secondary veins may or may not resume in lower lobes.

hydathod sites and concentration of free auxin (see Fig. 3) which determines the order and coordination of the developing veins.

5. Asymmetric affects in leaf vein structure during leaf growth

Our aim is to develop a measure of symmetry of the bifurcating structure of mature leaf veins. However, this asymmetry developmentally originated during the early stages of the leaf growth. Thus, we attempt to quantify the asymmetry introduced during the developmental stages of leaf growth based on the above described growth model. Although many factors and chemical substances are involved in the growth process, we simplify the model by considering only the affects on the vein structure of the asymmetries in concentration of auxin in the leaf margin.[1]

Consider the following cases of deviation from perfect symmetry based on the growth model (Fig. 3):

(1) Asymmetry in the auxin concentration in the stipules during the very early growth stages (Fig. 2A) and/or at the tip of the primordium (Fig. 2B). This asymmetry affects the

[1] It would be more efficient and reasonable to measure the concentration of auxin itself and the arising asymmetries therein during the growth stages. However, this is impractical in large leaf samples due to physical, technical, and biological limitations. Thus, we are restricted to measuring the affects of asymmetric auxin concentration as expressed in the final vein structure of the mature leaf.

acropetal growth of the mid-vein and induces an asymmetric or non-linear main vein. See Fig. 3A.

(2) Asymmetric concentration of free auxin along the leaf margin affects differentiation of secondary veins, which in turn induces asymmetric veins. We consider the following cases:
   (a) Asymmetry is expressed in the magnitude of the free auxin concentration while maintaining symmetry of concentration site (hydathod) position along the leaf margin. This induces asymmetry in the length of the secondary veins. See Fig. 3B.
   (b) Asymmetry is expressed in misalignment of auxin concentration sites, while maintaining equality of concentration magnitude. This induces asymmetric bifurcation points along the main vein. See Fig. 3C.
   (c) Asymmetry is expressed in free auxin concentration in both concentration site position along the leaf margin and in magnitude concentration. This induces secondary vein growth in asymmetric bifurcation points along the main vein, as well as asymmetry in length of these secondary veins. See Fig. 3D.

(3) Extreme asymmetry is expressed in the free auxin concentration site position and magnitude so as to produce no partnering secondary vein. Free auxin concentration points and magnitude may (or may not) recover to produce paired secondary veins in lower lobes of the leaf. This has the affect of creating a 'missing' secondary vein. See Fig. 3E.

6. Methods

6.1. Measuring symmetry of bifurcating structures

Given the growth model and the above described affects of asymmetry on the leaf vein structure, we define a class of bifurcating structures which generalizes the realizable structures manifested by the growth model. These structures are assumed to consist of a central main vein which is viewed as the symmetry axis, from which secondary veins bifurcate on both sides. Variations in this structure include differences in the number of secondary veins, their bifurcation points along the main vein, their lengths and their curvature. We concentrate on planar bifurcating structures representing veins of leaves. Fig. 6A shows a specimen with the vein structure marked.

Guided by the underlying biological processes, we define the measure of symmetry of a structure as the minimal amount of energy required to deform it into a symmetric structure. When measuring the symmetry of these structures, deformations are restricted to those consistent within the structure class. For clarity, we initially assume all veins are linear. Specifically, we assume the main vein is linear and serves as the symmetry axis. We also assume all secondary veins are linear and create a constant bifurcation angle with the main vein. We later extend the structure class and our approach to deal with curved veins.

In the following, we propose two approaches to quantify the asymmetry expressed in the leaf vein structures:

(1) *LoA* is based on evaluating the amount of deformation required to symmetrize the structure by applying a sequence of allowable elementary deformations.
(2) *GoA* is based on evaluating the amount of deformation required to symmetrize the structure by applying translation of all structure points at once.

Details of the two approaches are given in the following sections.

6.2. Measuring symmetry of bifurcating structures—LoA

Given a bifurcating structure such as a leaf vein structure, we find the minimum energy deformation which transforms it into a symmetric structure. Deformations consist of a series of permissible 'elementary' deformations. We restrict the 'elementary' deformations to three types of actions, motivated by the biological growth model of leaves (see Ref. [38] and Section 5):

(1) Insertion (deletion)—an additional secondary vein is added (deleted).
(2) Translation—a secondary vein is translated along the main vein.
(3) Elongation (contraction)—length of a secondary vein is changed.

Fig. 4 demonstrates these 'elementary' deformations. Any sequence of these elementary deformations maintains the structure within the class of bifurcating structures as defined in Section 3. Every elementary action is associated with a cost function which represents the energy required to perform the action. The energy of deforming a structure accumulates the cost of performing each 'elementary' deformation. The measure of symmetry of a structure is the cost of the minimum energy deformation that transforms the original structure into a symmetric structure.

We additionally impose a constraint inherent in the growth model [38], in which elementary deformations are applied such that the order of the secondary veins on either side of the main vein is preserved (i.e., there is no crossover when pairing left and right veins). This constraint is consistent with the growth model in which the secondary veins are created in the order in which free auxin concentration is created, which in turn is from the tip of the leaf and then sequentially along the leaf margin (see Section 4).

To find the minimum energy deformation, we represent the problem as a string matching problem [39]. For a given specimen the main vein is segmented into a large finite number of sections. The segmented vein is mapped into two vectors, the length of which is equal to the number of segments. The vectors describe the left and right bifurcating structure by assigning '0' to an entry if there is no secondary vein bifurcating out of the vein segment corresponding to that entry. A positive real value is assigned to the entry if there is such a bifurcation and

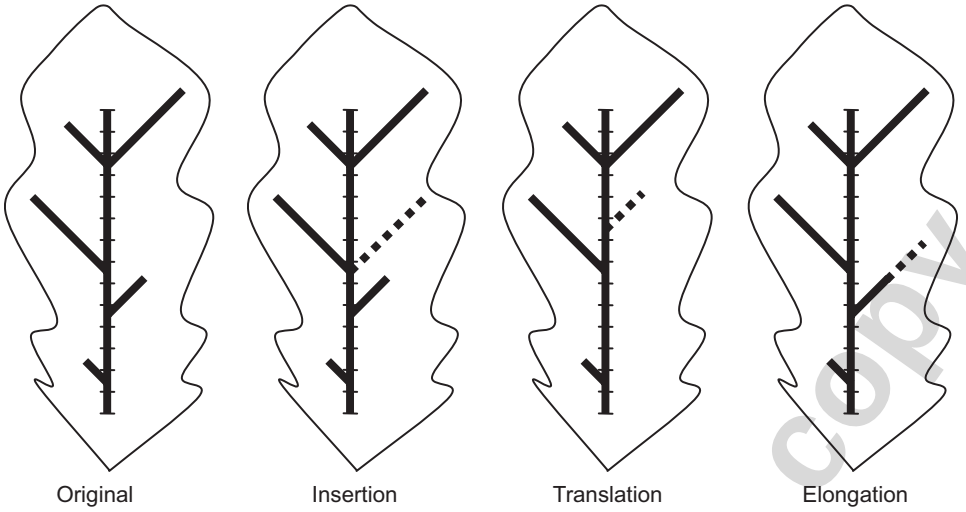

Fig. 4. Elementary deformations allowed in the LoA symmetry measure evaluation.

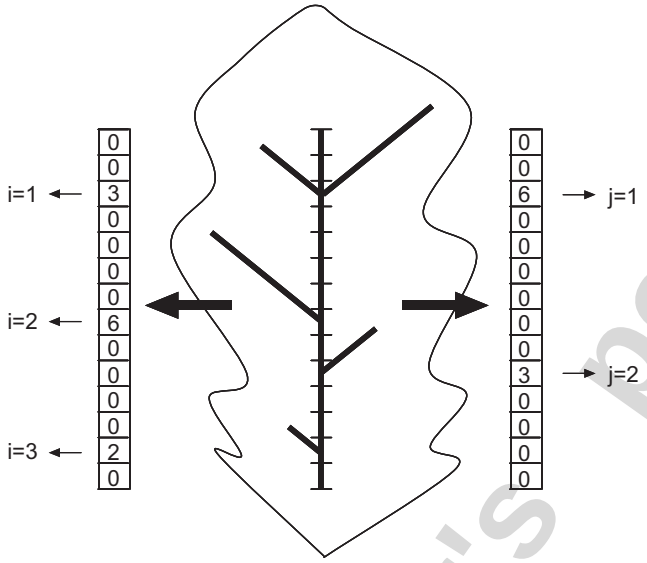

Fig. 5. Mapping a leaf structure into two vectors. The main vein of the leaf is segmented into a finite number of sections and mapped into two vectors. The vectors describe the left and the right bifurcating structure by assigning '0' to an entry if there is no secondary vein bifurcating out of the vein segment corresponding to that entry. A positive real value is assigned to the entry if there is such a bifurcation and the assigned value equals the length of the secondary vein.

the assigned value equals the length of the secondary vein. An example is shown in Fig. 5.

Finding the minimum energy deformation of the bifurcating structure is equivalent to finding the minimum cost of transforming one vector into the other, using allowed 'elementary' deformations. We solve this modified string matching problem using Dynamic Programming [39] as follows.

Let $i = 1 \ldots n$ enumerate the secondary veins on one side of the main vein (w.l.o.g. we assume the left side) and let $j = 1 \ldots m$ be the enumeration of the secondary veins on the other side (Fig. 5). Denote by $C_{i,j}$ the cost of the minimal energy deformation of the sub-structure consisting of the main vein and the first i secondary veins on the left and the first j secondary veins on the right.

The value of $C_{i,j}$ is given by one of the following possibilities:

1. Pair the left vein i with the right vein j. Thus $C_{i,j}$ equals $C_{i-1,j-1}$ plus the cost of translating veins i and j so that their positions align and the cost of equalizing the length of veins i and j.
2. Insert a new left vein as a pair for vein j. Thus $C_{i,j}$ equals $C_{i,j-1}$ plus the cost of inserting a new vein of length and position equal to vein j.
3. Insert a new right vein as a pair for vein i. Thus $C_{i,j}$ equals $C_{i,j-1}$ plus the cost of inserting a new vein of length and position equal to vein i.

It is easily shown that this recursive definition implies that $C_{n,m}$ is indeed an optimal solution which minimizes the cost function while observing the order constraint defined above. Calculating $C_{i,j}$ requires calculating the costs of solving the sub-problems $C_{i-1,j-1}$, $C_{i,j-1}$ and $C_{i-1,j}$, thus, the dynamic programming approach solves for the optimal solution in a bottom-up approach initialized with $C_{0,0} = 0$.

We start by defining the cost of the three elementary deformations:

$$COE(l, l_{new}) = E_0 * |l - l_{new}|,$$
$$COT(l, d) = T_0 * l * d,$$
$$COI(l) = I_0 * l,$$

where COE is the cost of elongating or shortening a vein of original length l to new length l_{new}. The cost of length change is invariant to the type of change (i.e., elongation or shortening). This cost function attempts to evaluate the asymmetry in free auxin concentration magnitude in the growing leaf which induces secondary veins of different lengths (see Section 5, and Fig. 3B). It is assumed that asymmetry increases with increase

in concentration magnitude difference, which in turn increases the difference in length of paired veins.

COT is the cost of translating a vein of length l by a distance of d units. The cost of length change is invariant to the direction of translation. This cost function attempts to evaluate the asymmetry in the free auxin concentration magnitude and position along the leaf margin which induces secondary veins of different lengths at different bifurcation points along the main vein (see Section 5, and Fig. 3D). The assumption is that asymmetry is larger, the greater the difference in concentration position and the greater the difference in concentration magnitude. Thus the *COT* is dependent on both length l and distance d.

COI is the cost of insertion of a vein of length l. The cost is invariant to the position of the vein along the main vein and to the side (left/right) in which insertion is performed. Cost of insertion is equal to cost of deletion, thus the latter is not used in the algorithm. This cost function attempts to evaluate the asymmetry in free auxin concentration when there is a missing concentration site which in turn implies a missing secondary vein (see Section 5, and Fig. 3E). Assumption is that asymmetry increases with increase in magnitude of the paired concentration site. Thus the *COI* is dependent on length l.

E_0, I_0 and T_0 are scalar weights determining the relative affects of each elementary deformation. Their values were set according to the biological growth model [38]. Since *COI* and *COE* both relate to quantification of asymmetry in concentration magnitude of paired sites, we assume that $I_0 = E_0$. *COT* quantifies asymmetry in both concentration magnitude and site positioning of paired sites, thus we have that T_0 serves as a balancing weight between the magnitude and positioning parameters. Typically $I_0 > T_0$.

Using these cost functions for elementary deformations, we define the following cost functions used in the algorithm:

$$COP_{i,j} = COT(min(length(i), length(j)), abs(pos(i) - pos(j))) + COE(length(i), length(j)),$$
$$COI_i = COI(length(i)),$$

where *COP* is the cost of pairing left vein i with right vein j. The cost consists of translating one of the veins towards the other and changing the length of one vein to that of the other. Since *COT* depends on the length of the vein, minimum cost is obtained when the shorter of the two veins is translated.

COI_i is the cost of inserting a new vein to be paired with vein i.

We now define the recursive cost function $C_{i,j}$ as follows:

$$\begin{cases} C_{i,j} = \min(C_{i-1,j-1} + COP_{i,j}, C_{i-1,j} + COI_j, C_{i,j-1} + COI_i), \\ C_{i,0} = \sum_{k=1}^{i} COI_k, \\ C_{0,j} = \sum_{k=1}^{j} COI_k, \\ C_{0,0} = 0. \end{cases}$$

The dynamic programming algorithm outputs the cost of the optimal solution $C_{n,m}$, which is defined as the measure of symmetry of the original bifurcating structure. In addition to the symmetry value, the sequence of elementary deformations used to obtain the optimal solution is run and a symmetrized version of the original structure is thus obtained.

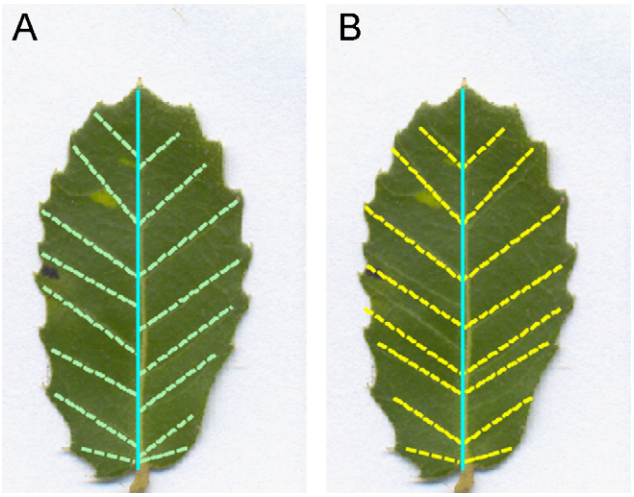

Fig. 6. Measuring asymmetry with the Local Approach (LoA). (A) Veins of the leaf are marked. (B) The resulting symmetric structure (produced by the local approach method). LoA = 1.6048.

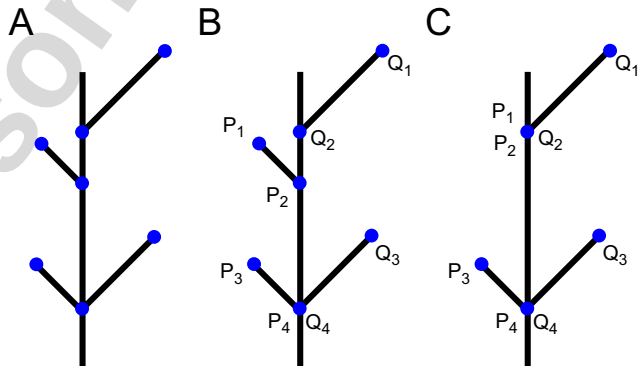

Fig. 7. Representation of bifurcating structure used in the global approach. (A) The bifurcating structure is viewed as a collection of points interconnected by segments. (B) Points P_k and Q_k on paired veins have been matched. (C) A new vein is inserted as points P_1 and P_2 (matching Q_1 and Q_2) which are the endpoints of the new vein. Points P_1, P_2 and Q_2 coincide.

To bound the run-time of the algorithm, observe that for $i, j \geqslant 2$ each value of $C_{i,j}$depends only on the values of $C_{i-1,j-1}$, $C_{i,j-1}$ and $C_{i-1,j}$. Therefore, computing $C_{n,m}$, requires the computation of all $C_{i,j}$ for $i \leqslant n$ and $j \leqslant m$ giving a total run-time of $O(mn)$.

We note that in order to obtain invariance to overall scale we normalize the original structures to have a norm of 1 prior to computing the symmetry distance.

Fig. 6A shows an example of a leaf with marked veins. The main vein is marked with a solid line and is considered as the symmetry axis of the structure. The secondary veins are marked with dashed lines. The resulting symmetric vein structure and the symmetry value are calculated according to the local approach and are shown in Fig. 6B.

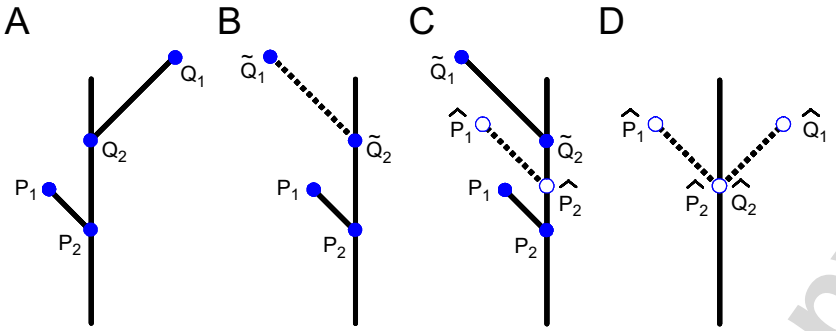

Fig. 8. Computing the CSM using the folding–unfolding method [37] applied to a pair of secondary veins, each represented by two points. (A) Original bifurcating structure with matching points marked. (B) Fold—Vein Q is reflected across the symmetry axis obtaining the folded points $\tilde{Q}_1$ and $\tilde{Q}_2$. (C) *Average*—The folded points are averaged with their matching points obtaining the points $\hat{P}_1$ and $\hat{P}_2$. (D) *Unfold*—The average points are reflected back across the symmetry axis obtaining the unfolded points $\hat{Q}_1$ and $\hat{Q}_2$. The CSM value is the average distance squared between the original points and the corresponding unfolded points: $\frac{1}{4}[(P_1-\hat{P}_1)^2+(P_2-\hat{P}_2)^2+(Q_1-\hat{Q}_1)^2+(Q_2-\hat{Q}_2)^2]$. The unfolded points form a symmetric configuration that is 'closest' to the original in terms of the average mean squared distance.

6.3. Measuring symmetry of bifurcating structures—GoA

Rather than separating into elementary deformations, this approach measures the amount of deformation required globally. This measure of symmetry is based on early work on Continuous Symmetry Measures (CSM) [37]. In these studies, symmetry is evaluated by estimating the energy (work) required to deform a non-symmetric configuration into a perfectly symmetric one.

In Refs. [6,7] symmetry of molecules was measured using the CSM approach, by allowing deformations that preserve the topology of the original structures. In this paper we allow deformations that do not necessarily preserve topological connectivity but that are consistent with biological models of the source structures (in our case veins of leaves). Specifically, in the case of our class of bifurcating structures, the main vein is constrained to form the symmetry axis, the secondary veins are constrained to bifurcate from the main vein, and secondary veins originating from two different bifurcation points along the main vein may deform so as to bifurcate at a common point.

In this approach, the bifurcating structure is viewed as a collection of points interconnected by segments (see Fig. 7A). The approach requires matching pairs of points to be deformed into symmetric pairs. In the case of our bifurcating structures, this pairing of points reduces to pairing of secondary veins. Fig. 7B shows an example where points on paired veins have been matched (point P_k matches point Q_k). In the case of a 'missing' secondary vein, an insertion of a new zero length vein is required which is marked as two endpoints located at the bifurcation point. Fig. 7C shows the paired points in such a case, where P_1 and P_2 are the endpoints of the new vein inserted as a match for Q_1 and Q_2, respectively. Since a pairing of the veins is required, the dynamic programming approach described in Section 6.2 can be exploited here as well. The cost function used in this case is based on the CSM:

$$COP_{i,j} = CSM(pointsonvein(i), pointsonvein(j)),$$
$$COI_i = CSM(pointsonvein(i), pointsonNullvein(i)),$$

where COP is the cost of pairing left vein i with right vein j. COI_i is the cost of inserting a new vein to be paired with vein i.

Given a paired set of veins (whether two existing veins or an inserted missing vein), the CSM of the pair of veins is computed by averaging the CSM value of each pair of matching points on these two veins.

$$CSM(P_r, Q_r) = \tfrac{1}{4}[(P_x - Q_x)^2 + (P_y - Q_y)^2],$$

where (P_x, P_y) are the 2D coordinates of point P and (Q_x, Q_y) are the 2D coordinates of point Q that has been reflected across the symmetry axis [37]. The computation of the CSM value can be visualized using the folding–unfolding method [37], as shown in Fig. 8. The symmetric bifurcating structure closest to the original is given as a byproduct of the CSM method (Fig. 8D).

Note that the CSM approach constrains the secondary vein end points along the main vein to remain positioned along the main vein. The approach allows veins to change length, translate bifurcation point and add additional veins to the structure. Thus the deformation applied by the CSM (and the folding–unfolding method) maintains the structure within the bifurcating structure class defined earlier.

As can be easily noticed the CSM calculations (and the folding–unfolding method) can be applied to all the veins simultaneously. It inherently involves both translation and elongation operations, hence the 'globality' of the approach.

As in the local approach, in order to obtain invariance to overall scale we normalize the original structures to have a norm of 1 prior to computing the symmetry distance.

Fig. 9A demonstrates an example of a leaf with marked veins. The main vein is marked with a solid line and is considered the symmetry axis of the structure. The secondary veins are marked with dashed lines. The resulting symmetric vein structure and the symmetry value are calculated according to the global approach and are shown in Fig. 9B.

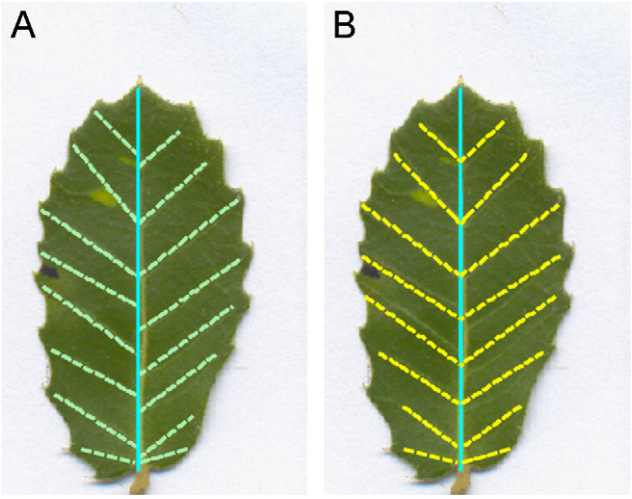

Fig. 9. Measuring symmetry using the global approach (GoA). (A) Veins of the leaf are marked. (B) The resulting symmetric structure. GoA = 0.59086.

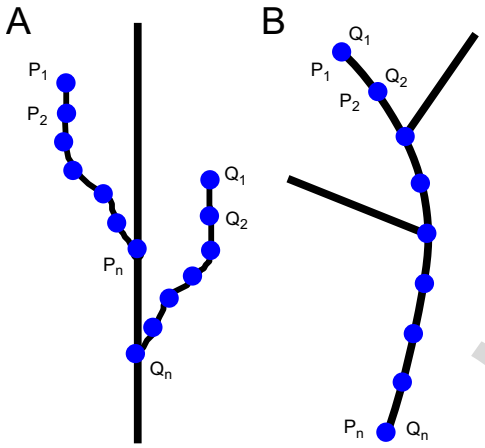

Fig. 10. Evaluating the CSM for curved bifurcating structures. The veins are sampled with a large (constant) number of points per vein. The CSM is calculated for each pair of matching points. (A) Secondary veins are sampled and matched. (B) A curved main vein is sampled by many points. Each point is considered as two aligned points that form a matching pair.

6.4. Extending the approach to curved bifurcating structures

The CSM approach extends naturally to deal with curved veins (both main vein and secondary veins). Rather than sampling only the endpoints of the vein, a larger (constant) number of sampling points are distributed along each vein (e.g., at equal distances). The points are paired as above and the CSM is computed for each pair (Fig. 10).

Note that for calculating the CSM and deforming the structure in the case of a curved main vein, points are sampled along the main vein such that each point is considered as a pair of matched points that are aligned (Fig. 10B).

Fig. 11A demonstrates an example of a leaf with marked veins. The main vein is marked with a solid line and is considered the symmetry axis of the structure. The secondary veins are marked with dashed lines. The resulting symmetric vein

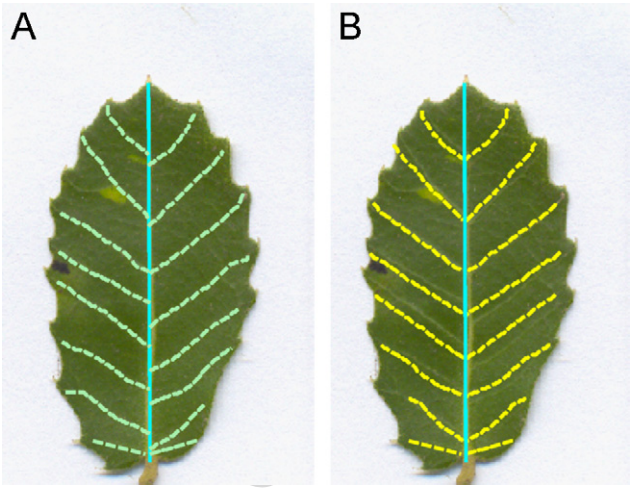

Fig. 11. Measuring symmetry using the extended Global Approach. (A) Veins of the leaf are marked. (B) The resulting symmetric structure. GoA = 0.64319.

structure and the symmetry value are calculated according to the extended global approach and shown in Fig. 11B.

7. Results

7.1. Consistency of performance

To test the performance of both the local and global methods we tested the algorithms on synthetic examples for which we systematically varied structure characteristics. Figs. 12 and 13 show synthetic examples from these tests:

1. Changing the distance along the main vein between paired veins (top row).
2. Changing the length of one of the paired veins (middle row).
3. Changing the number of unpaired veins (bottom row).

These figures show the consistency of both the local and global approach methods. Asymmetry measured by both these methods monotonically increases when these structure parameters vary and the system becomes less symmetric.

7.2. Experiments

The symmetry measure developed for bifurcating structures was exploited as part of an ongoing evolutionary study on stress, biodiversity evolution (reviews in Refs. [40–42]) and developmental stability (FA) [43,44] in the 'Evolution Canyon' (EC), lower Nahal Oren, mount Carmel, Israel (32°43′N; 34°58′E). The opposite slopes of the canyon display remarkable physical and biotic contrasts at the microscale. Although located only a few hundred meters apart and sharing the same macroclimatic zone, similar rock and soil, the microclimatic conditions on the slopes vary dramatically; affecting the biology of organisms at all levels. The south-facing slopes (SFS) may receive as much as up to 200–800% more solar radiation than the north-facing slopes (NFS). Consequences of higher radiation include higher temperature, higher luminance and lower humidity [45]. Thus,

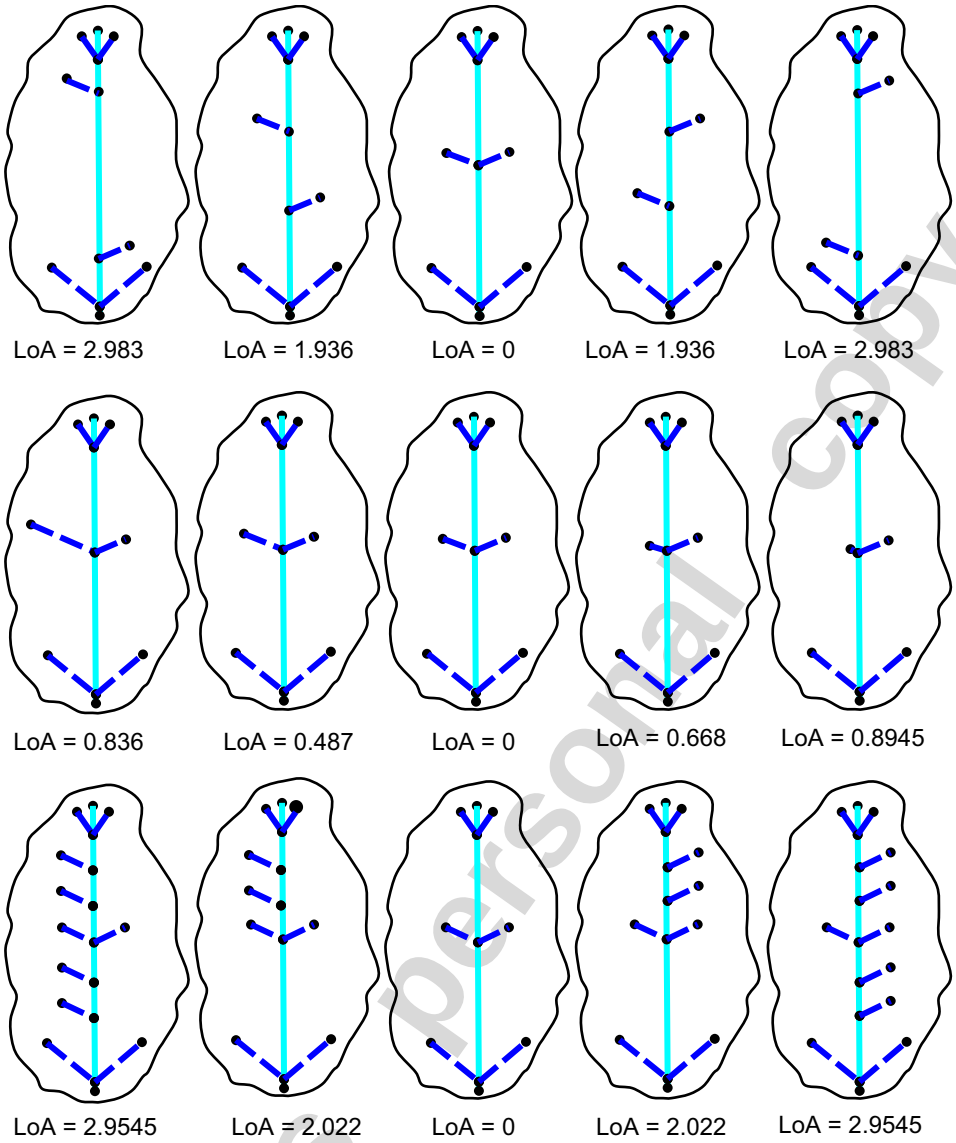

Fig. 12. Consistency of the Local Approach (LoA) under systematic changes in structure characteristics. 1. Changing the distance along the main vein between paired veins (top row). 2. Changing the length of one of the paired veins (middle row). 3. Changing the number of unpaired veins (bottom row).

the 'African' like SFS has a more xeric environment, that is, warmer, drier and a more variable microclimate, than the mesic 'European' like NFS slope.

In our experiment we focus on *Quercus calliprinos*, which is the most common local tree. Its large population on the NFS demands more mesic conditions and lower temperature than those appearing on the SFS, although a small population does exist on this slope [45].

We analyzed 201 *Q. calliprinos* leaves, 101 from the NFS and 100 from the SFS. Ten leaves were sampled from 10 different trees in each one of the slopes. Sampling was conducted on a single day in February 2004. Leaves were scanned, and the middle vein and secondary veins, were marked in the digital image. In this work we show that the symmetry measure of bifurcating structures applied to the veins of leaves shows the deviation from perfect symmetry as caused by the deviation from normal environmental conditions. This correlation is shown using classification. We show that classifying a novel specimen based on both local and global measures improves classification of the specimen to its correct environment over classification based on classic, well-known symmetry measures [12,14,46].

7.2.1. Building the classifier

We build a classifier that discriminates between samples of the SFS and the NFS of the canyon. The classifier is based on the support vector machine classifier (SVM) [47]. The SVM is a tool for classifying data into two sets. The SVM consists of two phases: the training phase and the testing phase. In the training phase the SVM receives a large number of samples belonging to each of the two groups (the quantity of samples from the two sets need not be equal). Each sample is represented by a feature vector. The classifier builds a rule of distinction between the two sets based on the feature vectors of these examples.

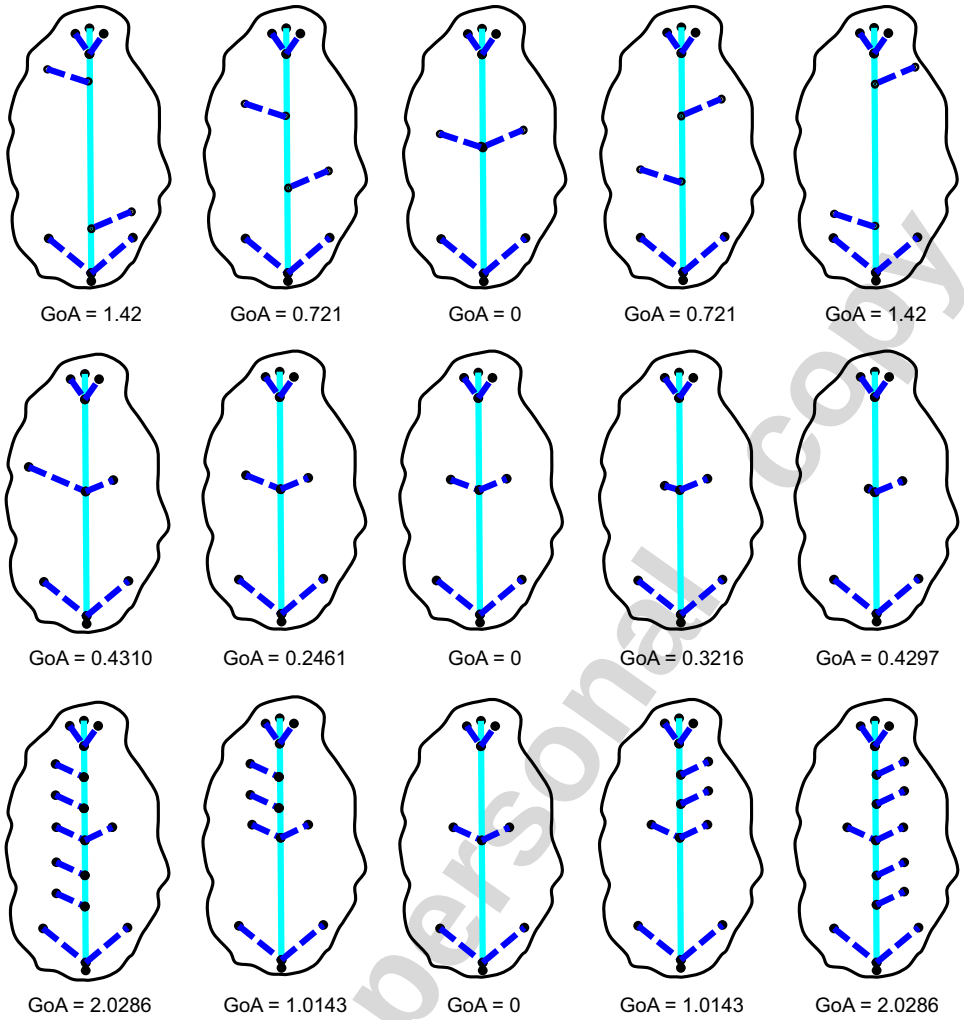

Fig. 13. Consistency of the Global Approach (GoA) under systematic changes in structure characteristics. 1. Changing the distance along the main vein between paired veins (top row). 2. Changing the length of one of the paired veins (middle row). 3. Changing the number of unpaired veins (bottom row).

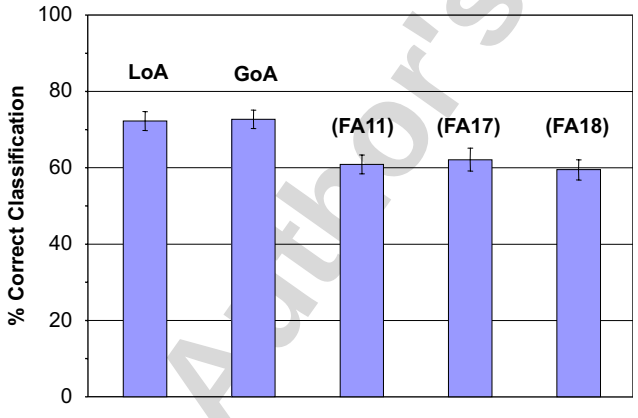

Fig. 14. Comparing classification performance using different measures of symmetry. Our local approach (LoA) and global approach (GoA), are shown in comparison to classic symmetry measures of Leary [48] (FA11), Strobeck [12] (FA17), and Klingenberg [14] (FA18). Hundred and one leaves from the 'European' NFS and 100 leaves from the 'African' SFS were used in our tests. Each test was run 500 times. Error bars represent standard deviation. One can easily see that both our measures improve separation ability. The Local Approach improves classification by 16.25% and the Global Approach improves classification by 19%.

The rule might be based on a linear model, a quadratic model, etc. In the testing phase the SVM classifier receives a novel specimen and grades its association with one of the two sets based on the rule of distinction determined in the training phase.

Due to the small number of examples we adopted the V-fold cross validation method for testing the quality of classification [48]. This method allows increasing the number of samples by combining the various subsets of existing data. Thus, different, randomly chosen subsets of the SFS and NFS samples were used for training the SVM. Samples not included in these subsets were then used as test cases to evaluate classification. This process was repeated 500 times with different subsets of the same size. The classifier was trained and then tested using various combinations of the following features (see review and comparison of these features in Ref. [12]):

(1) LoA—Our symmetry value based on the local approach.
(2) GoA—Our symmetry value based on the global approach.
(3) FA11 index of Leary et al. [46]. Sums over differences of traits between left and right sides of an individual.

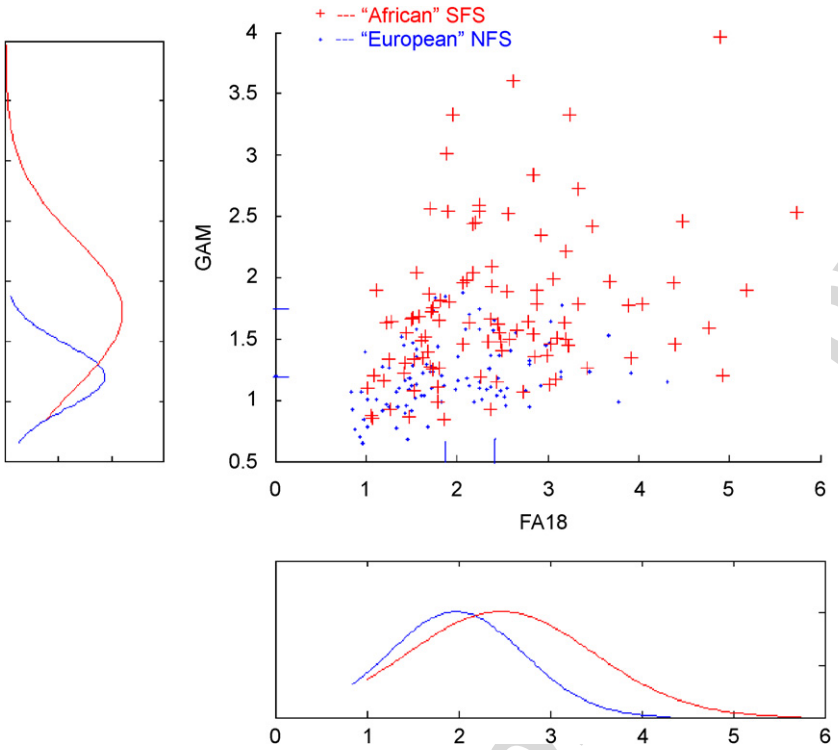

Fig. 15. Visualizing the separation capabilities of the classic symmetry measure of Klingenberg (FA18) vs that of our Global Symmetry (GoA). Every point in the diagram represents a single specimen. 'European' NFS specimens are marked by blue dots. 'African' SFS specimens are marked by red crosses. Statistical distributions of the symmetry values are shown below and beside the plot. It is easily seen that the GoA measure provides a higher separation between the two classes compared to FA18. In the latter case the mean of the 'European' NFS and the mean of the 'African' SFS are almost congruent and are both of large variance. Whereas the means as well as the variance of the 'European' NFS and 'African' SFS distributions of GoA values differ significantly and allow better separation.

(4) FA17 index of Strobeck [12]. Averages over the traits of the logarithms of differences between left and right sides of an individual.
(5) FA18 index of Klingenberg [14]. Sums differences between coordinates of landmarks of left and right sides of an individual.

The percentage of correct classifications was determined in each case. The weights used for the LoA computation (Section 6.2) were optimal weights for this classification and were determined using a gradient descent approach. The parameters used were $T0 = 1$, $I0 = E0 = 154$. The GoA approach does not rely on any parameters.

In all our experiments we used the SVM with linear kernels.

7.3. Classification results

Average results of classification using the global approach measure, the local approach method, FA11, FA17, and FA18 measures separately are shown in Fig. 14. Classification using combinations of these measures can be found in Appendix A. Comparing to three well-known biological multi-trait symmetry measures [46,12,14] one can easily see that both our methods improve the separation performance of the classification. The local approach improves by around 16% and the global approach improves by around 19%. Combining the local approach and the global approach methods does not yield improvement over classification based on each measure separately. Fig. 15 visualizes the difference in separation ability between the classic symmetry measure of Klingenberg (FA18) and our Global Measure (GoA).

8. Conclusion

We proposed a measure of symmetry for bifurcating structures, namely leaf veins, which is based on biological growth models. It is based on geometric as well as topological properties of the structures. The measure quantifies the amount of energy required to deform the structure into a perfectly symmetric one. Deformation is restricted to 'elementary' actions which are in accord with biological growth models.

We introduce two computational schemes to calculate the symmetry measure, and show the consistency of the measure with various deformations as well as its effectiveness in both classifying leaves taken from plants growing under different stress conditions and comparing it with other leading methods. The obtained results show clearly that our measures which are based on the minimum energetic path underlying biological mechanisms yield better separation ability.

Acknowledgments

We thank Vladimir Frenkel for his comments on the manuscript, Roni Aloni and Avigdor Beiles for providing

stimulating discussions of some of the issues rose in the article and Liah Shatz for assistance in field work.

Appendix A.

Table 1 shows the classification results using all combinations of the five symmetry measures described in Section 7.2.1.

The combinations are denoted as 5-bit notation vectors. The entries in the vector represent (left to right): The Local Measure (LoA), the Global Measure (GoA), FA11, FA17 and FA18. The measures used in a specific classification test are marked by 1 in the appropriate entry of the notation vector. (For example, [01011] represents the combination of measures: GoA, FA17 and FA18).

Table 2 shows the classification results using all combinations of the Local approach measure, Global approach measure and Palmer's measure of single traits (FA2) [12].

The combinations are denoted as 3-bit notation vectors. The entries in the vector represent (left to right): The Local Measure (LoA), the Global Measure (GoA) and FA2. The measures used in a specific classification test are marked by 1 in the appropriate entry of the notation vector. (For example, [011] represents the combination of measures: GoA and FA2).

Table 1
Classification results using combinations of symmetry measures (multiple traits)

Notation vector	Percent correct classification	Standard deviation
[1 0 0 0 0]	72.2281	2.4554
[0 1 0 0 0]	72.6945	2.4356
[0 0 1 0 0]	60.8674	2.4905
[0 0 0 1 0]	62.1324	2.994
[0 0 0 0 1]	59.4894	2.6497
[1 1 0 0 0]	71.0776	2.7538
[1 0 1 0 0]	70.6603	2.7755
[1 0 0 1 0]	72.215	2.7912
[1 0 0 0 1]	71.8239	2.7068
[0 1 1 0 0]	71.9385	2.5984
[0 1 0 1 0]	73.4097	2.8403
[0 1 0 0 1]	72.7011	2.8266
[0 0 1 1 0]	61.2781	2.96
[0 0 1 0 1]	62.4646	3.3084
[0 0 0 1 1]	62.3337	3.0934
[1 1 1 0 0]	70.9418	2.5011
[1 1 0 1 0]	71.9401	2.9759
[1 1 0 0 1]	70.9827	2.7126
[1 0 1 1 0]	71.0826	3.2259
[1 0 1 0 1]	71.166	2.8006
[1 0 0 1 1]	71.3526	2.8711
[0 1 1 1 0]	72.8222	2.9978
[0 1 1 0 1]	71.9074	2.9112
[0 1 0 1 1]	72.6455	3.0683
[0 0 1 1 1]	61.6938	3.1126
[1 1 1 1 0]	71.8992	2.8541
[1 1 1 0 1]	71.4164	2.8167
[1 1 0 1 1]	71.2969	2.9311
[1 0 1 1 1]	71.1562	3.1334
[0 1 1 1 1]	72.2789	3.1606
[1 1 1 1 1]	71.909	2.8004

Table 2
Classification results using combinations of symmetry measures (single traits)

Notation vector	Percent correct classification	Standard deviation
[1 0 0]	72.2281	2.4554
[0 1 0]	72.6945	2.4356
[0 0 1]	70.8887	2.4562
[1 0 1]	74.2721	2.5994
[0 1 1]	75.1731	2.6363
[1 1 1]	74.9448	2.5755

One can see that in the case of single traits both our measures, LoA and GoA, do improve separation by 4.77% and 6.04% correspondingly.

References

[1] H. Weyl, Symmetry, Princeton University Press, Princeton, NJ, 1952.
[2] M. Gardner, The new ambidextrous universe—symmetry and asymmetry from mirror reflections to superstrings, W.H. Freeman and Company, New York, 1979.
[3] H. Zabrodsky, D. Weinshall, Using bilateral symmetry to improve 3D reconstruction from image sequences, Comput. Vision Image Understanding 67 (1997) 48–57.
[4] H. Ishikawa, D. Geiger, R. Cole, Finding tree structures by grouping symmetries, ICCV, 2005, pp. 1132–1139.
[5] L. Babai, Isomorphism testing and symmetry of graphs, Ann. Discrete Math. 8 (1980) 101–109.
[6] H. Zabrodsky, D. Avnir, Continuous symmetry measures, J. Am. Chem. Soc. 114 (1992) 7843–7851.
[7] H. Zabrodsky, S. Peleg, D. Avnir, Continuous symmetry measures ii: Symmetry groups and the tetrahedron, J. Am. Chem. Soc. 115 (1993) 8278–8289.
[8] L. Van Valen, A study of fluctuating asymmetry, Evolution 16 (1962) 125–142.
[9] A. Moller, J. Swaddle, Asymmetry, Developmental Stability, and Evolution Oxford Series in Ecology and Evolution, Oxford, 1997.
[10] A. Palmer, C. Strobeck, Fluctuating asymmetry: measurement, analysis, patterns, Ann. Rev. Ecol. Syst. 17 (1986) 391–421.
[11] A. Palmer, C. Strobeck, Fluctuating asymmetry analyses: a primer, in: Developmental Instability: Its Origins and Evolutionary Implications, vol. 199, Kluwer Academic Publishers, Dordrecht, 1994, pp. 335–364.
[12] A. Palmer, C. Strobeck, Fluctuating asymmetry analyses revisited, in: Developmental Instability (DI): Causes and Consequences, Oxford, 2003, pp. 279–213.
[13] B. Leung, M. Forbes, D. Houle, Fluctuating asymmetry as a bioindicator of stress: comparing efficacy of analyses involving multiple traits, Am. Nat. 155 (2000) 101–115.
[14] C. Klingenberg, G. McIntyre, Geometric morphometrics of developmental instability: analyzing patterns of flactuating asymmetry with Procrustes methods, Evolution 52 (1998) 1363–1375.
[15] C. Klingenberg, M. Barluenga, A. Meyer, Shape analysis of symmetric structures: quantifying variation among individuals and asymmetry, Evolution 56 (2002) 1909–1920.
[16] R. Aloni, K. Schwalm, M. Langhans, C. Ullrich, Gradual shifts in the sites of free-auxin production during leaf-primordium development and their role in vascular differentiation and leaf morphogenesis in Arabidopsis, Planta 216 (2003) 841–853.
[17] R. Aloni, Foliar and axial aspects of vascular differentiation-hypotheses and evidence, J. Plant Growth Regul. 20 (2001) 22–34.
[18] M. Atallah, On symmetry detection, IEEE Trans. Comput. 34 (1985) 663–673.

[19] J. Wolter, T. Woo, R. Volz, Optimal algorithms for symmetry detection in two and three dimensions, Visual Comput. 1 (1985) 37–48.
[20] P. Highnam, Optimal algorithms for finding the symmetries of a planar point set, Inform. Process. Lett. 22 (1985) 219–222.
[21] H. Alt, K. Mehlhorn, H. Wagener, E. Welzl, Congruence, similarity, and symmetry of geometric objects, Discrete Comput. Geom. 3 (1988) 237–256.
[22] P. Saint-Marc, G. Medioni, B-Spline contour representation and symmetry detection, in: First European Conference on Computer Vision, 1990, pp. 604–606.
[23] A. Kuehnle, Symmetry based recognition of vehicle rears, Pattern Recognition Lett. 12 (1991) 249–258.
[24] H. Ogawa, Symmetry analysis of line drawings using the Hough transform, Pattern Recognition Lett. 12 (1991) 9–12.
[25] S. Dinggang, H. Horace, K. Kent, K. Eam, Symmetry detection by generalized complex moments: a close-form solution, IEEE Trans. Pattern Anal. Mach. Intell. 21 (1999) 466–476.
[26] Y. Hel-Or, S. Peleg, H. Zabrodsky, How to Tell Right from Left, Conference on Computer Vision and Pattern Recognition, 1988.
[27] M. Kazhdan, B. Dobkin, A. Finkelstein, T. Funkhouser, A reflective symmetry descriptor, European Conference on Computer Vision, vol. 2, 2002, pp. 642–656.
[29] P. Minovic, S. Ishikawa, K. Kato, Symmetry identification of a 3-D object represented by octree, IEEE Trans. Pattern Anal. Mach. Intell. 15 (1993) 507–514.
[30] C. Sun, J. Sherrah, 3D symmetry detection using the extended Gaussian image, IEEE Pattern Anal. Mach. Intell. 19 (1997) 164–168.
[31] M. Kazhdan,T. Funkhouser, S. Rusinkiewicz, Rotation invariant spherical harmonic representation of 3D shape descriptors, Symposium on Geometry Processing, 2003.
[32] C. Sun, Symmetry detection using gradient information, Pattern Recognition Lett. 14 (1995) 987–996.
[33] G. Marola, On the detection of the axes of symmetry of symmetric and almost symmetric planar images, IEEE Pattern Anal. Mach. Intell. 11 (1989) 104–108.
[34] T. Zielke, M. Brauckmann, W. Von Seelen, Intensity and edge based symmetry detection with application to car following, CVGIP: Image Understanding, vol. 58, 1993, pp. 177–190.
[35] J. Bigun, Recognition of Local Symmetries in Grey Value Images by Harmonic Functions, IEEE Computer Society Press, Silver Spring, MD, 1988, pp. 345–347.
[36] A. Buda, K. Mislow, A Hausdorff chirality measure, J. Am. Chem. Soc. 114 (1992) 6006–6012.
[37] H. Zabrodsky, S. Peleg, D. Avnir, Symmetry as a continuous feature, IEEE Trans. Pattern Anal. Mach. Intell. 17 (1995) 1154–1166.
[38] R. Aloni, I. Cornelia, Free auxin production and vascular differentiation in Arabidopsis leaves, Plant Physiol. (essay) 19.5 (2005).
[39] T. Cormen, C. Leiserson, R. Rivest, C. Stein, Introduction to Algorithms, The MIT Press, Cambridge, 2001.
[40] E. Nevo, Asian African and European biota meet at 'Evolution Canyon' Israel: Local tests of global biodiversity and genetic diversity patterns, Proc. R. Soc. Lond B 262 (1995) 149–155.
[41] E. Nevo, Evolution in action across phylogeny caused by microclimatic stresses at 'Evolution Canyon', Theoret. Popul. Biol. 52 (1997) 231–243.
[42] E. Nevo, Evolution of genome–phenome diversity under environmental stress, Proc. Natl. Acad. Sci. USA 98 (2001) 6233–6240.
[43] M. Auslander, E. Nevo, M. Inbar, The effects of slope orientation on plant growth, developmental instability and susceptibility to herbivores, J. Arid Environ. 55 (2003) 405–416.
[44] E. Derzhavets, A. Korol, E. Nevo, Differences in fluctuating asymmetry in Drosophila melanogaster caused by microclimatic contrasts, Drosophila Inform. Service (1997) 73–80.
[45] T. Pavliceck, D. Sharon, V. Kravchenko, H. Saaroni, E. Nevo, Microclimatic interslope differences underlying biodiversity contrasts in evolution canyon, Mt. Carmel Israel Isr, J. Earth Sci. 51 (2003) 55–57.
[46] R. Leary, F. Allendorf, K. Knudsen, Developmental instabillity and high meristic counts in interspecific hybrids of salmoid fishes, Evolution 39 (1985) 1318–1326.
[47] V. Vapnik, The Nature of Statistical Learning Theory, Springer, New York, 1995.
[48] P. Burman, A comparitive study of ordinary cross-validation, v-fold cross-validation and repeated learning-testing methods, Biometrika 76 (1989) 503–514.

About the Author—DAVID MILNER received his M.Sc. degree in Mathematics and Computer Sciences from The University of Haifa. His interests are in the area of computer vision, mathematical modeling and algorithms.

About the Author—SHMUEL RAZ is currently studying towards his M.Sc. degree in evolutionary Biology in the Department of Environmental and Evolutionary Biology, Institute of Evolution at The University of Haifa. His research interests are in fluctuating asymmetry as a Bioindicator of stress and fluctuating asymmetry heritability.

About the Author—HAGIT HEL-OR is a faculty member in the Department of Computer Science at the University of Haifa. She earned her degrees at the Hebrew University of Jerusalem. Her research area is in the field of Imaging Science and Technologies and includes Color Vision, Image Processing, Computational and Human Vision.

About the Author—DANIEL KEREN is a faculty member in the Department of Computer Science at the University of Haifa. He earned his Ph.D. degree at the Hebrew University of Jerusalem. His research areas include Image processing and Computer Vision.

About the Author—EVIATAR NEVO is the director of the Institute of Evolution, at The University of Haifa, Israel and is a foreign associate to the National Academy of Sciences, U.S.A. He earned his degrees, in biology, from the Hebrew University of Jerusalem, Israel. His research interests include the origin of species and adaptations in nature and the maintenance of genetic diversity in natural populations of plants and animals.